inorganics

MDPI

Article

Size-Activity Relationship of TiO_2-Supported Pt Nanoparticles in Hydrogenation Reactions

Qi Zhang [1,†], Tianbo Li [1,*,†], Xiang-Ting Min [2,*], Shu-Xian Li [2], Xunzhu Jiang [2], Qian Zhang [2], Yangyang Li [2], Xinlong Yan [1], Rui Feng [1], Feifei Yang [1], Wei Zhou [1], Xiaoyan Hu [1], Botao Qiao [2] and Zhonghai Ni [1]

[1] School of Chemical Engineering and Technology, China University of Mining and Technology, Xuzhou 221116, China; ts22040058a31@cumt.edu.cn (Q.Z.); yanxl@cumt.edu.cn (X.Y.); fengrui@cumt.edu.cn (R.F.); feiyang@cumt.edu.cn (F.Y.); zhouwei@cumt.edu.cn (W.Z.); huxiaoyan@cumt.edu.cn (X.H.); nizhonghai@cumt.edu.cn (Z.N.)
[2] CAS Key Laboratory of Science and Technology on Applied Catalysis, Dalian Institute of Chemical Physics, Chinese Academy of Sciences, Dalian 116023, China; lishuxian@dicp.ac.cn (S.-X.L.); xzjiang@dicp.ac.cn (X.J.); zqq872211@dicp.ac.cn (Q.Z.); liyangyang@dicp.ac.cn (Y.L.); bqiao@dicp.ac.cn (B.Q.)
* Correspondence: litianbo@cumt.edu.cn (T.L.); minxiangting@dicp.ac.cn (X.-T.M.)
† These authors contributed equally to this work.

Abstract: Quantitative assessments of the geometric influence on catalytic activity are crucial for catalyst design and understanding reaction mechanisms. In this study, we synthesized a series of catalysts comprising TiO_2-supported Pt nanoparticles with varying particle sizes, which were systematically evaluated in representative hydrogenation reactions. A consistent size–activity relationship is established, wherein overall turnover frequency (TOF) values ($TOF_{overall}$: calculated as moles of reactant converted per mole of Pt per hour) are modeled as functions of the average diameter of the supported Pt particles, yielding slope values consistently near −1 across a variety of common substrates. This finding underscores that catalytic activity predominantly originates from surface sites on the Pt nanoparticles rather than from interfacial, edge, or corner active sites.

Keywords: catalytic hydrogenation; size–activity relationship; geometric influence; nanocatalysis; hydrogen spillover

check for updates

Academic Editors: Antonino Gulino and Agnieszka Feliczak-Guzik

Received: 28 March 2025
Revised: 23 May 2025
Accepted: 30 May 2025
Published: 6 June 2025

Citation: Zhang, Q.; Li, T.; Min, X.-T.; Li, S.-X.; Jiang, X.; Zhang, Q.; Li, Y.; Yan, X.; Feng, R.; Yang, F.; et al. Size-Activity Relationship of TiO_2-Supported Pt Nanoparticles in Hydrogenation Reactions. *Inorganics* **2025**, *13*, 186. https://doi.org/10.3390/inorganics13060186

Copyright: © 2025 by the authors. Licensee MDPI, Basel, Switzerland. This article is an open access article distributed under the terms and conditions of the Creative Commons Attribution (CC BY) license (https://creativecommons.org/licenses/by/4.0/).

1. Introduction

Hydrogenation is among the central themes of the petrochemical, coal chemical, and fine chemical industries. For example, in the petrochemical industry, processes like hydroreforming and hydro-isomerization are pivotal for enhancing the octane value of gasoline, while the hydrogenation of benzene to cyclohexane is a critical step in the production of nylon intermediates. Noble metals are extensively employed in these hydrogenation reactions due to their exceptional catalytic activity. However, given the high cost and limited availability of noble metals, there is an urgent need to develop highly active and efficient catalysts for hydrogenation reactions. In past research, a widely accepted yet simplified notion is that smaller noble metal nanoparticles yield higher overall activity per unit of noble metal loading [1,2]. Consequently, researchers have shown great interest in strategies to reduce the size of supported noble metal nanoparticles and to elucidate the catalytic performance differences arising from size variation, emphasizing the essential need to understand the structure–activity relationship [3–5].

Current studies on the structure–activity relationship in the hydrogenation of supported noble metal catalysts primarily focus on the selectivity of nanoparticles of different

sizes or provide nonquantitative insights into how nanoparticle diameter affects catalytic activity [2,4,6]. Notable examples include hydrogenation reactions such as cinnamyl aldehyde hydrogenation [7–9], ethene semi-hydrogenation [10–13], and nitroaromatic hydrogenation [5,14–27]. However, detailed quantitative investigations into the relationship between nanoparticle size and catalytic activity remain scarce. Given the frequent comparisons of catalytic performance across nanoparticles of varying sizes in heterogeneous hydrogenation catalysis, we highlight the urgent need for rigorous quantitative evaluations to clarify the geometric influence on catalytic activity.

Quantitatively described size–activity relationships in catalytic reactions, such as CO oxidation and low-temperature water–gas shift (LWGS), have been elegantly demonstrated by the groups of M. Cargnello and M. Shekhar [28–31], respectively. By theoretical simulation and CO oxidation catalyzed by CeO_2-supported metal, the groups of M. Cargnello correlated the ceria–metal interface sites with slope of overall turnover frequency (TOF) and the size of supported metal particles (unless otherwise specified, all TOF values refer to the overall TOF, calculated as moles of reactant converted per mole of Pt per hour). Concretely speaking, the overall TOF calculated based on all metal located on support and catalyst dispersion was put aside. Then, the slope value of the linear fitting equation of l n (overall TOF) and l n (metal size) should correspond with which part active catalytic sites are located. Inspired by these pioneering studies, we sought to adopt analogous analytical paradigms to elucidate the geometric influence on catalytic activity in representative hydrogenation reactions. Herein, we synthesized a series of TiO_{22}-supported Pt nanoparticles with systematically varied particle sizes and rigorously evaluated their performance across representative hydrogenation reactions. A robust size–activity relationship was observed, with turnover frequency (TOF) values modeled as functions of the average diameter of the Pt nanoparticles, consistently yielding slope values near -1 across a range of common substrates. These findings highlight that catalytic activity is predominantly derived from surface sites on the Pt nanoparticles rather than from interfacial, edge, or corner sites, offering new insights into the fundamental structure–activity relationship in these systems.

2. Results

In this work, a series of catalysts consisting of TiO_2-supported Pt nanoparticles with average sizes of approximately 2.32 nm, 4.38 nm, 9.63 nm, 14.64 nm, and 40.98 nm were synthesized (details provided in the Supporting Information). Inductively coupled plasma optical emission spectrometry (ICP-OES) analysis indicated Pt loading rates of approximately 1 wt% for all prepared Pt/TiO_2 catalysts (detailed data provided in Table S1). These average sizes were determined from transmission electron microscopy (TEM) images, with representative TEM images shown in Figure 1 (additional images are available in Figure S1). Each size variant was supported on TiO_2 and labeled accordingly: 2-Pt/TiO_2, 4-Pt/TiO_2, 10-Pt/TiO_2, 15-Pt/TiO_2, and 41-Pt/TiO_2. In addition, the TEM images revealed similar sub-globular shapes for the supported Pt nanoparticles across the series. In addition, attempts to further determine the particle sizes by X-ray diffraction (XRD) (Figure 2) were unsuccessful owing to the low Pt loading. All five nanoparticle size fractions, each displaying sub-spherical Pt morphology, were prepared by the same polyol colloidal route under identical surfactant and reduction conditions, and TEM and XRD confirm the absence of sintering necks or irregular aggregates in every sample.

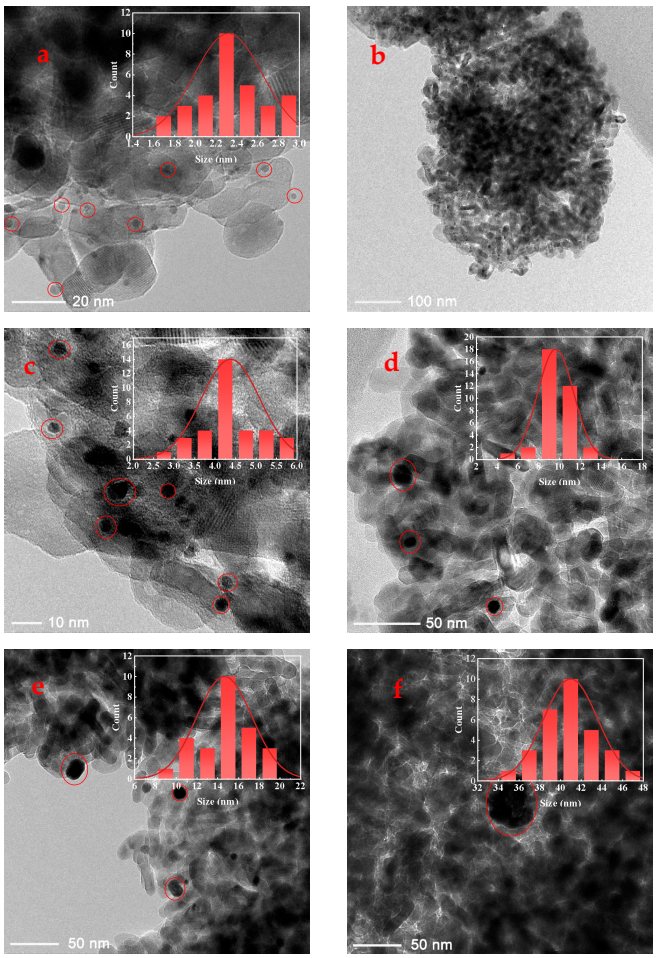


Figure 1. TEM images and particle size statistical results of 2-Pt/TiO_2 (**a**) and (**b**), 4-Pt/TiO_2 (**c**), 10-Pt/TiO_2 (**d**), 15-Pt/TiO_2 (**e**) and 41-Pt/TiO_2 (**f**) catalysts, respectively.

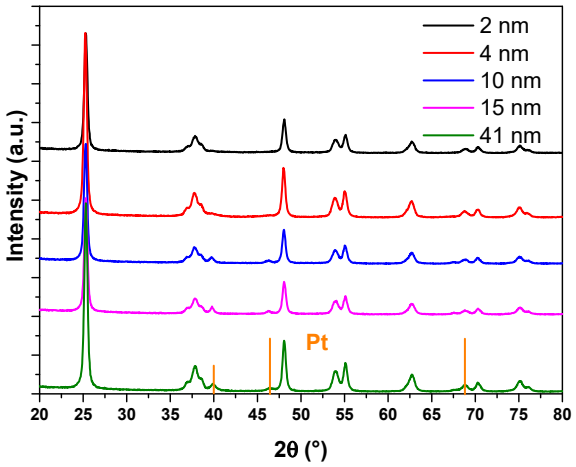


Figure 2. XRD characterization of 2-Pt/TiO_2, 4-Pt/TiO_2, 10-Pt/TiO_2, 15-Pt/TiO_2 and 41-Pt/TiO_2 catalysts.

Nitrobenzene hydrogenation is a fundamental catalytic reaction with broad applications in fine chemical production. Numerous studies have explored Pt-based catalysts for this transformation, underscoring their efficacy and versatility [27,32–34]. In this work, we evaluated the performance of the synthesized Pt/TiO_2 catalysts in nitrobenzene hydrogenation using H_2.

Hydrogenation experiments were systematically conducted under varying reaction conditions using 4-Pt/TiO_2 as the initial catalyst. Initial control experiments using TiO_2 as the catalyst confirmed its inactivity for the reaction, as no conversion was observed even after 6 h (Table 1, entry 1). In sharp contrast, the introduction of Pt nanoparticles onto the TiO_2 support markedly enhanced catalytic activity, achieving approximately 21% conversion within just 1 h (Table 1, entry 2). Interestingly, a moderate increase in reaction temperature to 30 °C (Table 1, entry 3) further boosted the conversion to 31%, with a concomitant rise in the turnover frequency (TOF) from 669.8 h^{-1} (Table 1, entry 1) to 1012.8 h^{-1}. However, as the reaction temperature was increased further (Table 1, entries 4 and 5), the incremental improvements in TOF became less pronounced, suggesting a saturation effect at higher temperatures. Prolonging the reaction time to enhance the conversion (Table 1, entry 6) led to a significant decrease in TOF. This decline is likely attributed to kinetic limitations arising from substrate depletion during the later stages of the reaction.

Table 1. Performance of 4-Pt/TiO_2 at various reaction conditions for nitrobenzene hydrogenation.

Entry [a]	Temp. (°C)	Time (h)	Conv. (%)	TOF (h^{-1})
1 [b]	25	6	0	/
2	25	1	20.7	669.8
3	30	1	30.6	1012.8
4	35	1	34.2	1044.0
5	40	1	35.2	1145.5
6	25	3	59.8	644.1

[a] Reaction conditions: nitrobenzene, 1 mmol; 10 mL ethanol; 5 mg 4-Pt/TiO_2 catalyst; H_2 pressure, 0.1 MPa. [b] 5 mg TiO_2 support was used. TOF values refer to the overall TOF, calculated as moles of reactant converted per mole of Pt per hour.

Based on the above findings, a reaction temperature of 25 °C was selected for further studies. At this temperature, the conversion of nitrobenzene remains sufficiently low, minimizing the impact of substrate depletion on the reaction rate. Additionally, the mild conditions are expected to enhance the stability of the supported Pt catalyst, ensuring prolonged performance with high reliability. Reusability tests were conducted with the 4-Pt/TiO_2 catalyst, and no significant loss in overall TOF was observed after five consecutive cycles, as illustrated in Figure 3. These results demonstrate the robustness and stability of the catalyst under the chosen reaction conditions.

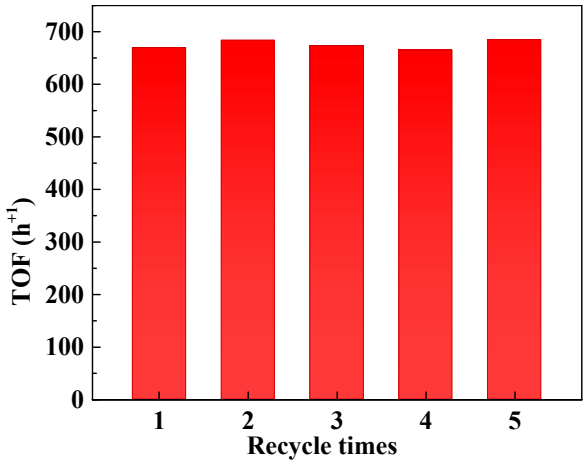


Figure 3. Catalyst recycling experiment. Reaction conditions: nitrobenzene, 1 mmol; 10 mL ethanol; 5 mg 4-Pt/TiO_2 catalyst; H_2 pressure, 0.1 MPa; reaction time, 1 h. TOF values refer to the overall TOF, calculated as moles of reactant converted per mole of Pt per hour.

A qualitative relationship between the apparent reaction rate and Pt nanoparticle size was observed, indicating that the overall TOF decreased as the average Pt particle diameter increased, the trend shown in Table 2. To ensure the nitrobenzene conversion remained sufficiently low and comparable across all entries in Table 2, thereby equalizing the impact of reaction kinetics on TOF calculations, the reaction times were adjusted accordingly. Therefore, the reaction times of 2-Pt/TiO_2 and 4-Pt/TiO_2, 10-Pt/TiO_2, 15-Pt/TiO_2 and 41-Pt/TiO_2 are increased with the overall TOF reduced.

Table 2. Performance of NPs Pt with different average sizes supported by TiO_2 for hydrogenation of nitrobenzene [a].

Entry	Catalyst	Time (h)	Conv. (%)	TOF (h^{-1})
1	2-Pt/TiO_2	1	22.7	718.3
2	4-Pt/TiO_2	1	20.7	669.8
3	10-Pt/TiO_2	2	10.7	184.1
4	15-Pt/TiO_2	5	16.2	108.1
5	41-Pt/TiO_2	5	9.0	62.2

[a] Reaction conditions: nitrobenzene, 1 mmol; solvent, 10 mL ethanol, 5 mg catalyst; temperature, 25 °C; H_2 pressure, 0.1 MPa. TOF values refer to the overall TOF, calculated as moles of reactant converted per mole of Pt per hour.

Building on the model proposed by Matteo Cargnello, which establishes a quantitative relationship between overall TOF and different supported crystalline metal grains with uniform packing structures, we developed a simplified version to create a highly generalized reference framework that facilitates direct comparison. In this generalized model, logical deduction (details provided in the Supporting Information) demonstrates that the natural logarithm of the overall TOF and the natural logarithm of the supported metal particle diameter form a linear relationship. The slope of this linear function is directly linked to the distribution of active sites on the supported metal particles. Specifically, slope values of −1, −2, and −3 correspond to surface active sites, interfacial/edge active sites, and corner active sites, respectively. Using this simplified model, we applied logarithmic transformations to the TOF data from Table 2, treating TOF as the dependent variable and the average Pt particle diameter as the independent variable. Employing linear regression to plot the experimental data, the slope was determined to be approximately −1, as shown in Figure 4. This result suggests that the active sites on Pt particles are predominantly located on their surface.

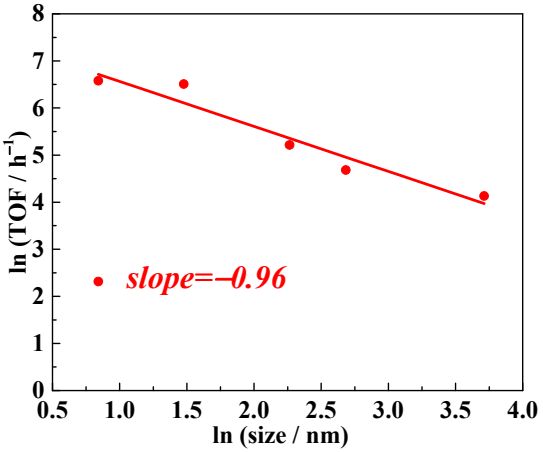


Figure 4. Nitrobenzene hydrogenation activity of NPs Pt with different average sizes supported by TiO_2. TOF values refer to the overall TOF, calculated as moles of reactant converted per mole of Pt per hour.

It should be noted that this inference is based on necessary but reasonable assumptions, which are crucial for the generalized model we proposed before. Supported crystalline metal grains should present similar figures and uniform packing structures even if the size changes. In addition, active sites that are located in the same kind of areas on Pt particles, to be more specific, including surface parts, interfacial/edge parts, or corner parts, should perform uniform or approximate activity, respectively. However, the assumption about uniform activity might correspond to all cases. Here is a typical counterexample reported that for CH_4 reactions with CO_2 or H_2O over supported Pt clusters, CH_4 turnover rates over surface Pt sites are different on Pt clusters with different sizes [3]. These two hypotheses may narrow the range of applicability but significantly enhance reliability. Fortunately, the CO-DRIFTS results shown in Figure 5 indicate that the Pt nanoparticles in this study exhibit relatively uniform adsorption behavior, supporting the rationale and necessity for the assumptions of uniform shape and activity. Linear CO adsorption signals were observed between 2000 and 2100 cm^{-1}, with peaks around 2088 cm^{-1} and 2065 cm^{-1} corresponding to CO adsorption on $Pt^{\delta+}$ and Pt^0 sites, respectively. Similar adsorption signals have been reported for other Pt-based catalysts [35,36], further validating these findings.

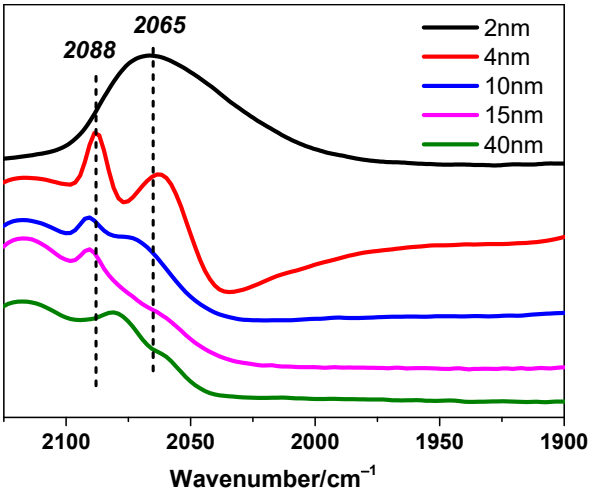


Figure 5. CO-DRIFTS for Pt/TiO_2 catalysts. 2-Pt/TiO_2 (black), 4-Pt/TiO_2 (red), 10-Pt/TiO_2 (blue), 15-Pt/TiO_2 (pink), and 41-Pt/TiO_2 (green).

XPS analyses were also carried out, and peak–deconvolution of the Pt 4f region (Figure 6) shows virtually identical binding energies for both metallic Pt^0 ($4f7/_2 \approx 71.2$ eV) and the slightly oxidized $Pt^{\delta+}$ component ($4f7/_2 \approx 72.0$ eV) across all Pt/TiO_2 catalysts. This uniform valence–state distribution further substantiates our assumption of consistent particle morphology and comparable per-site activity.

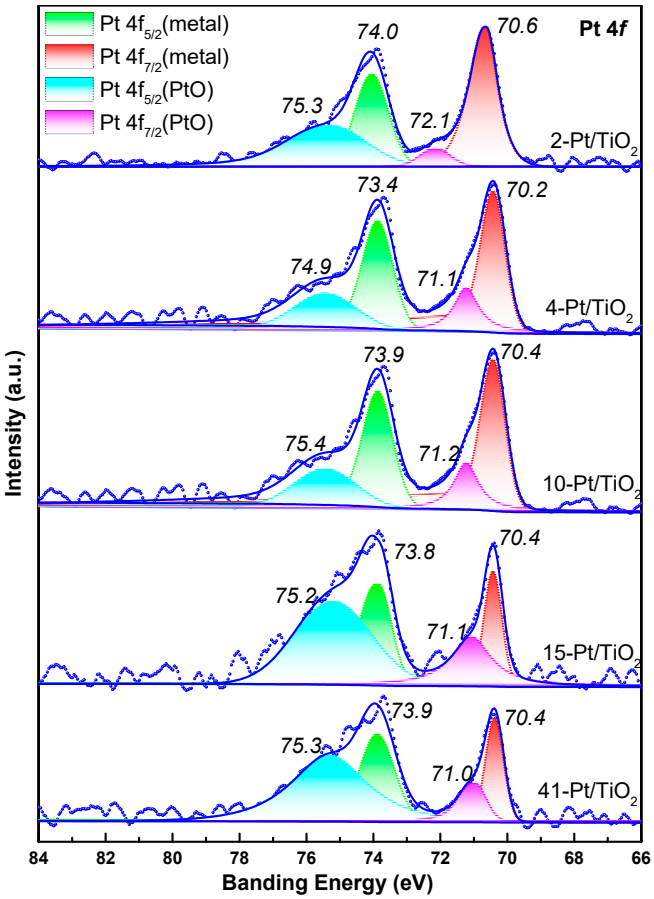


Figure 6. XPS and results of peak–differentiating and imitating for Pt/TiO_2 catalysts.

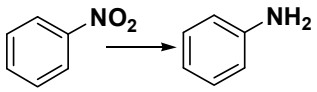
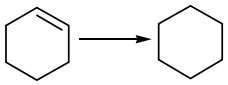
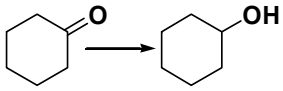
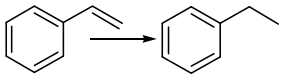
3. Discussion

To delve deeper, we propose that the dominant factor influencing catalyst performance in this work is the activation of H_2 or substrates on the surface sites of Pt nanoparticles rather than the spillover of H_2 or H atoms from Pt to TiO_2. Literature reports suggest two common hydrogenation mechanisms for heterogeneous catalytic processes: direct hydrogenation and hydrogen spillover [37–43]. While it is challenging to exclude the coexistence of these two mechanisms in the hydrogenation reactions catalyzed by Pt/TiO_2, certain inferences can be made. Hydrogen spillover involves the migration of hydrogen atom equivalents from metal nanoparticles to the support, implying that the interfacial sites between the Pt surface and TiO_2 would serve as the active sites if spillover were the dominant mechanism. In such a case, the slope value of the linear relationship between TOF and Pt particle diameter would be expected to be −2. However, this is inconsistent with the experimental results for nitrobenzene hydrogenation. Instead, the observed slope value, approximately −1, suggests that surface sites on the Pt nanoparticles are the primary active sites (Figure 4). Thus, we conclude that the dominant parameter governing catalyst performance in this work is the activation of H_2 or substrates on these surface sites rather than hydrogen spillover.

Considering the universality of the slope description for the size–activity relationship of Pt nanoparticles supported on TiO_2, we extended the study to other typical unsaturated substrates, including cyclohexene, cyclohexanone, and styrene, under similar reaction conditions. Typical results are collected and shown in Table 3. Following logarithmic transformation and linear regression analysis of the experimental data (raw data provided in Tables S1–S4), the results, shown in Figure 7, revealed slope values close to −1, −0.87, −1.18, and −0.85 for cyclohexene, cyclohexanone, and styrene, respectively. These findings

indicate that, for the hydrogenation of these typical unsaturated substrates, the active sites are located on the surface of the supported Pt nanoparticles, consistent with our inference for nitrobenzene hydrogenation.

Table 3. Performance of 4-Pt/TiO_2 for various substrate hydrogenations. [a].

Entry	Reaction	Conv. (%)	TOF (h^{-1})
1		20.7	669.8
2		23.5	508.3
3		26.1	372.1
4		17.4	1071.4

[a] Reaction conditions details in Tables S2–S4. TOF values refer to the overall TOF, calculated as moles of reactant converted per mole of Pt per hour.

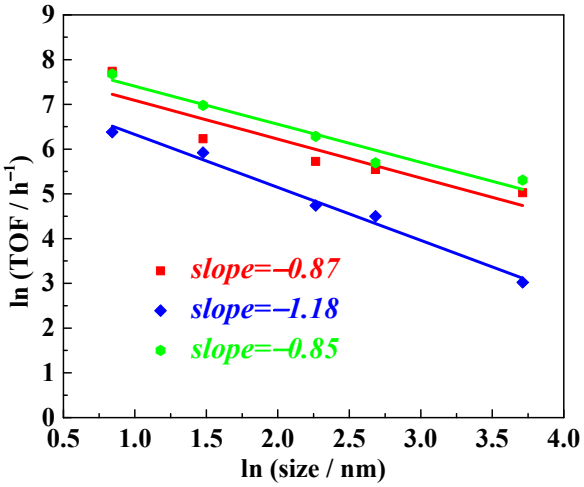


Figure 7. Cyclohexene (red), cyclohexanone (blue), and styrene (green) hydrogenation activity of NPs Pt with different sizes. TOF values refer to the overall TOF, calculated as moles of reactant converted per mole of Pt per hour.

4. Materials and Methods

4.1. Preparation of the H_2PtCl_6 Aqueous Solution

Dissolve the purchased H_2PtCl_6 in deionized water (DIW) to obtain H_2PtCl_6 aqueous solution.

4.2. Preparation of the 2-Pt/TiO_2 Catalyst

Measure 600 µL DIW and 600 µL H_2PtCl_6 aqueous solution into a test tube. Add 1 g TiO_2 after fully mixing the solution into the test tube. Ultrasound for 0.5 h, quiet for 6 h, then dry the test tube in an oven. After the solid is dried, burn it in a muffle furnace at 400 °C for 5 h. Then, place the solid in a reaction vessel and add 10 mL ethanol, fill with 1.0 MPa hydrogen, and reduce it for 1 h at 200 °C. Obtain a 2-Pt/TiO_2 catalyst after centrifugation and vacuum drying.

4.3. Preparation of the 4-Pt/TiO_2 Catalyst

Add 1 g TiO_2 and 100 mL DIW to the beaker. Add 100 mL DIW, 1 g of PVP, and 600 μL H_2PtCl_6 aqueous solution to the other beaker. Put the beaker into a water bath at 20 °C, turn on the magnetic stirring, and add 20 mL of aqueous solution containing 0.0102 g $NaBH_4$ slowly. Then, pour the suspension from the previous beaker into this beaker. Stir for 12 h. After filtration, washing, and drying, burn the solid in a muffle furnace at 400 °C for 5 h. Then, place the solid in a reaction vessel and add 10 mL of ethanol, fill with 1 Mpa hydrogen, and reduce it for 1 h at 200 °C. Obtain 4-Pt/TiO_2 catalyst after centrifugation and vacuum drying.

4.4. Preparation of the 10-Pt/TiO_2 Catalyst

Add 1 g TiO_2, 600 μL H_2PtCl_6 aqueous solution, 600 μL formaldehyde, and 100 mL DIW to the flask. Put the flask into oil bath at 120 °C, and stir for 12 h. After filtration, washing, and drying, burn the solid in a muffle furnace at 400 °C for 5 h. Then, place the solid in a reaction vessel and add 10 mL ethanol, fill with 1.0 MPa hydrogen, and reduce it for 1 h at 200 °C. Obtain 10-Pt/TiO_2 catalyst after centrifugation and vacuum drying.

4.5. Preparation of the 15-Pt/TiO_2 Catalyst

Add 1 g TiO_2, 600 μL H_2PtCl_6 aqueous solution, 600 μL formaldehyde, and 100 mL DIW to the flask. Put the flask into oil bath at 120 °C, and stir for 24 h. After filtration, washing, and drying, burn the solid in a muffle furnace at 400 °C for 5 h. Then, place the solid in a reaction vessel and add 10 mL of ethanol, fill with 1.0 MPa hydrogen, and reduce it for 1 h at 200 °C. Obtain 15-Pt/TiO_2 catalyst after centrifugation and vacuum drying.

4.6. Preparation of the 41-Pt/TiO_2 Catalyst

Add 1 g TiO_2, 600 μL H_2PtCl_6 aqueous solution, and 10 mL ethanol to the reaction kettle, fill with 1 Mpa hydrogen and reduce it for 1 h at 200 °C. After filtration, washing, and drying, burn the solid in a muffle furnace at 400 °C for 5 h. Then, place the solid in a reaction vessel and add 10 mL of ethanol, fill with 1 Mpa hydrogen, and reduce it for 1 h at 200 °C. Obtain 41-Pt/TiO_2 catalyst after centrifugation and vacuum drying.

4.7. Catalytic Performance

The nitrobenzene hydrogenation was conducted in a branched reaction tube equipped with a magnetic bar. In a typical procedure, 5 mg catalyst, 1 mmol nitrobenzene, and 10 mL ethanol were subjected to the branched reaction, which was then flushed with 1 atm H_2 five times and charged successively with 0.1 MPa H_2. After the branched reaction was sealed, it was placed in water bath at 25 °C. After reaction, 150 μL anisole was added to 5 mL the reaction liquid as inner standard. The product was qualitatively analyzed by gas chromatography (GC) and quantitatively analyzed on an Agilent 6890B instrument equipped with an on-column injector (250 °C), an FID detector (250 °C), and an HP-5 capillary column (30 m × 0.32 mm × 0.25 mm). The conversion was calculated by gas chromatography.

The cyclohexene hydrogenation was conducted in a branched reaction tube equipped with a magnetic bar. In a typical procedure, 5 mg catalyst, 1 mmol cyclohexene, and 10 mL ethanol were subjected to the branched reaction, which was then flushed with 1 atm H_2 five times and charged successively with 0.1 MPa H_2. After the branched reaction was sealed, it was placed in water bath at 25 °C. After reaction, 150 μL anisole was added to 5 mL the reaction liquid as inner standard. The product was qualitatively analyzed by gas chromatography (GC) and quantitatively analyzed on an Agilent 6890B instrument equipped with an on-column injector (250 °C), an FID detector (250 °C), and an HP-

5 capillary column (30 m × 0.32 mm × 0.25 mm). The conversion was calculated by gas chromatography.

The cyclohexanone hydrogenation was conducted in an autoclave equipped with a magnetic bar. In a typical procedure, 5 mg catalyst, 1 mmol cyclohexene, and 10 mL ethyl acetate were subjected to the autoclave, which was then flushed with 1 MPa H_2 five times and charged successively with 1 MPa H_2. After the autoclave was sealed, it was heated to 120 °C. After reaction, 150 μL benzaldehyde was added to 5 mL the reaction liquid as inner standard. The product was qualitatively analyzed by gas chromatography (GC) and quantitatively analyzed on an Agilent 6890B instrument equipped with an on-column injector (250 °C), an FID detector (250 °C), and an HP-5 capillary column (30 m × 0.32 mm × 0.25 mm). The conversion was calculated by gas chromatography.

The styrene hydrogenation was conducted in a branched reaction tube equipped with a magnetic bar. In a typical procedure, 5 mg catalyst, 1 mmol styrene, and 10 mL ethanol were subjected to the branched reaction, which was then flushed with 1 atm H_2 five times and charged successively with 0.1 MPa H_2. After the branched reaction was sealed, it was placed in water bath at 25 °C. After reaction, 150 μL anisole was added to 5 mL the reaction liquid as inner standard. The product was qualitatively analyzed by gas chromatography (GC) and quantitatively analyzed on an Agilent 6890B instrument equipped with an on-column injector (250 °C), an FID detector (250 °C) and an HP-5 capillary column (30 m × 0.32 mm × 0.25 mm). The conversion was calculated by gas chromatography.

The conversion of nitrobenzene was calculated as follows:

$$C = \frac{N_{an}}{N_{ni}} \times 100\%$$

The conversion of cyclohexene was calculated as follows:

$$C = \frac{N_{ca}}{N_{ce}} \times 100\%$$

The conversion of cyclohexanone was calculated as follows:

$$C = \frac{N_{cl}}{N_{co}} \times 100\%$$

The conversion of styrene was calculated as follows:

$$C = \frac{N_{et}}{N_{st}} \times 100\%$$

where N_{an}, N_{ni}, N_{ca}, N_{ce}, N_{cl}, N_{co}, N_{et}, and N_{st} represent mole amounts of aniline, nitrobenzene, cyclohexane, cyclohexene, cyclohexanol, acyclohexanone, ethylbenzene, and styrene, respectively.

The TOF refers to the overall TOF, calculated as moles of reactant converted per mole of Pt per hour was calculated as follows:

$$TOF = \frac{\text{Conversion of reaction substrate}}{\text{time} \times \text{Mole ratio of Pt/substrate}} \times 100\%$$

(6) Logical deduction about l n (TOF)-l n (size of NP Pt):

There are several premise assumptions:

I. Supported crystalline metal grains should present similar figures and uniform packing structure even if size changes.

II. Active sites that are located in the same kind of areas on Pt particles, to be more specific, including surface parts, interfacial/edge parts, or corner parts, should perform uniform or approximate activity, respectively.

For a certain Pt particle,

$N_V = \lambda_V \times V_{Pt} = \lambda_{V'} \times R^3$

$Ns = \lambda_S \times S_{Pt} = \lambda_{S'} \times R^2$

$N_I = \lambda_I \times P_{Pt} = \lambda_{I'} \times R$

$N_C = \lambda_C = \lambda_{I'} \times R^0$

If active sites located at surface part,

then $TOF_{real} = TOF_{overall} \times N_V / Ns = \lambda'_{V/S} \times TOF_{overall} \times R$,

$\ln TOF_{overall} = \ln (TOF_{real}/\lambda_{V/S}/R) = \lambda_{S0} - \ln R$,

so the slope about l n(TOF)−l n (size of NP Pt) is −1.

If active sites located at interfacial/edge part,

then $TOF_{real} = TOF_{overall} \times N_V/N_I = \lambda'_{V/I} \times TOF_{overall} \times R^2$,

$\ln TOF_{overall} = l\,n\ (TOF_{real}/\lambda_{V/I}/R) = \lambda_{I0} - 2\ln R$,

so the slope about l n (TOF)−l n (size of NP Pt) is −2.

If active sites located at corner part,

then $TOF_{real} = TOF_{overall} \times N_V/N_C = \lambda'_{V/C} \times TOF_{overall} \times R^3$,

$\ln TOF_{overall} = l\,n\ (TOF_{real}/\lambda_{V/C}/R) = \lambda_{C0} - 3\ln R$,

so the slope about l n (TOF)−l n (size of NP Pt) is −3.

N_V, Ns, N_I, and N_C are Pt atom numbers counted for volume of Pt particle, surface part of Pt particle, interfacial/edge part of Pt particle, and corner part of Pt particle, respectively. V_{Pt} is volume of supported Pt particle. S_{Pt} is surface area of supported Pt particle. P_{Pt} is perimeter part contacted with support of supported Pt particle. $\lambda_{XX}{}^X$ are constants related to figures of Pt particles and size of a single Pt atom.

5. Conclusions

In conclusion, uniform, size-controlled Pt NPs from 2 to 40 nm were synthesized, and corresponding supported catalysts were used in certain typical hydrogenations. A consistent size–activity relationship can be summarized when overall TOF was modeled as a function of supported metal particles' average diameter; the slope value of these functions is close to −1 consistently for a variety of common substrates. This size–activity relationship suggests that active sites are located at the surface part of supported Pt particles. A further inference is that the parameter that dominates the performance of the catalyst should not be hydrogen spillover from Pt nanoparticles to TiO_2 support for these typical hydrogenations. This study briefly but fittingly demonstrates the quantitative size–activity relationship of nanoparticle Pt supported by TiO_2 in certain typical hydrogenations, which might contribute to the design of related catalysts and research on other size–activity relationships of supported nanoparticle metals in heterogeneous catalysis.

Supplementary Materials: The following supporting information can be downloaded at: https://www.mdpi.com/article/10.3390/inorganics13060186/s1.

Author Contributions: Q.Z. (Qi Zhang): Experiment and Data Analysis. T.L.: Methodology, Data Analysis, and Writing. X.-T.M.: Writing and Editing. All other authors analyzed the experimental results and took part in discussions on manuscript preparation. All authors have read and agreed to the published version of the manuscript.

Funding: This work was financially supported by the National Key Research and Development Program of China (2021YFA1500503), the National Natural Science Foundation of China (22102210, 22302199, 22378079, 21961142006), and the Innovation and Entrepreneurship Doctor Program of Jiangsu Province (JSSCBS20211208).

Institutional Review Board Statement: Not applicable for studies not involving humans or animals.

Informed Consent Statement: Not applicable.

Data Availability Statement: The datasets analyzed or generated during this study are available from the authors.

Conflicts of Interest: The authors declare no conflicts of interest.

References

1. Liang, S.; Hao, C.; Shi, Y. The Power of Single-Atom Catalysis. *ChemCatChem* **2015**, *7*, 2559. [CrossRef]
2. Zhang, L.; Zhou, M.; Wang, A.; Zhang, T. Selective Hydrogenation over Supported Metal Catalysts: From Nanoparticles to Single Atoms. *Chem. Rev.* **2020**, *120*, 683. [CrossRef]
3. Wei, J.; Iglesia, E. Mechanism and Site Requirements for Activation and Chemical Conversion of Methane on Supported Pt Clusters and Turnover Rate Comparisons among Noble Metals. *J. Phys. Chem. B* **2004**, *108*, 4094. [CrossRef]
4. Kuhn, J.N.; Huang, W.; Tsung, C.-K.; Zhang, Y.; Somorjai, G.A. Structure Sensitivity of Carbon—Nitrogen Ring Opening: Impact of Platinum Particle Size from below 1 to 5 nm upon Pyrrole Hydrogenation Product Selectivity over Monodisperse Platinum Nanoparticles Loaded onto Mesoporous Silica. *J. Am. Chem. Soc.* **2008**, *130*, 14026. [CrossRef] [PubMed]
5. Zhu, Z.; Tao, H.; Zhou, Y. Using Density Functional Theory To Unravel the Size-Dependent Effect of Au Nanoparticles and Au Single Atoms Adsorbed on Carbon Nitride for the Hydrogenation of Nitrobenzene. *ACS Appl. Nano Mater.* **2022**, *5*, 18753. [CrossRef]
6. Vilé, G.; Albani, D.; Almora-Barrios, N.; López, N.; Pérez-Ramírez, J. Advances in the Design of Nanostructured Catalysts for Selective Hydrogenation. *ChemCatChem* **2016**, *8*, 21. [CrossRef]
7. Meemken, F.; Baiker, A. Recent Progress in Heterogeneous Asymmetric Hydrogenation of C=O and C=C Bonds on Supported Noble Metal Catalysts. *Chem. Rev.* **2017**, *117*, 11522. [CrossRef] [PubMed]
8. Bhogeswararao, S.; Srinivas, D. Intramolecular selective hydrogenation of cinnamaldehyde over CeO_2–ZrO_2-supported Pt catalysts. *J. Catal.* **2012**, *285*, 31. [CrossRef]
9. Cao, Z.; Bu, J.; Zhong, Z.; Sun, C.; Zhang, Q.; Wang, J.; Chen, S.; Xie, X. Selective hydrogenation of cinnamaldehyde to cinnamyl alcohol over BN-supported Pt catalysts at room temperature. *Appl. Catal. A Gen.* **2019**, *578*, 105. [CrossRef]
10. Guo, Y.; Huang, Y.; Zeng, B.; Han, B.; Akri, M.; Shi, M.; Zhao, Y.; Li, Q.; Su, Y.; Li, L.; et al. Photo-thermo semi-hydrogenation of acetylene on Pd_1/TiO_2 single-atom catalyst. *Nat. Commun.* **2022**, *13*, 2648. [CrossRef]
11. Guo, Y.; Qi, H.; Su, Y.; Jiang, Q.; Cui, Y.-T.; Li, L.; Qiao, B. High Performance of Single-atom Catalyst Pd_1/MgO for Semi-hydrogenation of Acetylene to Ethylene in Excess Ethylene. *ChemNanoMat* **2021**, *7*, 526. [CrossRef]
12. Tiwari, G.; Sharma, G.; Verma, R.; Gakhad, P.; Singh, A.K.; Polshettiwar, V.; Jagirdar, B.R. Acetylene Semi-Hydrogenation at Room Temperature over Pd—Zn Nanocatalyst. *Chem. A Eur. J.* **2023**, *29*, e202301932. [CrossRef] [PubMed]
13. Yang, L.; Guo, Y.; Long, J.; Xia, L.; Li, D.; Xiao, J.; Liu, H. PdZn alloy nanoparticles encapsulated within a few layers of graphene for efficient semi-hydrogenation of acetylene. *Chem. Commun.* **2019**, *55*, 14693. [CrossRef]
14. Sun, S.; Du, M.; Zhao, R.; Jv, X.; Hu, P.; Zhang, Q.; Wang, B. Zn(0)-Catalysed mild and selective hydrogenation of nitroarenes. *Green Chem.* **2020**, *22*, 4640. [CrossRef]
15. Li, M.; Chen, S.; Jiang, Q.; Chen, Q.; Wang, X.; Yan, Y.; Liu, J.; Lv, C.; Ding, W.; Guo, X. Origin of the Activity of Co–N–C Catalysts for Chemoselective Hydrogenation of Nitroarenes. *ACS Catal.* **2021**, *11*, 3026. [CrossRef]
16. Shi, H.; Dai, X.; Liu, Q.; Zhang, T.; Zhang, Y.; Shi, Y.; Wang, T. Magnetic CuNi Alloy Nanoparticles for Catalytic Transfer Hydrogenation of Nitroarene. *Ind. Eng. Chem. Res.* **2021**, *60*, 16011. [CrossRef]
17. Ishikawa, H.; Nakatani, N.; Yamaguchi, S.; Mizugaki, T.; Mitsudome, T. Robust Ruthenium Phosphide Catalyst for Hydrogenation of Sulfur-Containing Nitroarenes. *ACS Catal.* **2023**, *13*, 5744. [CrossRef]
18. Yang, F.; Wang, M.; Liu, W.; Yang, B.; Wang, Y.; Luo, J.; Tang, Y.; Hou, L.; Li, Y.; Li, Z.; et al. Atomically dispersed Ni as the active site towards selective hydrogenation of nitroarenes. *Green Chem.* **2019**, *21*, 704. [CrossRef]
19. Hajdu, V.; Muránszky, G.; Nagy, M.; Kopcsik, E.; Kristály, F.; Fiser, B.; Viskolcz, B.; Vanyorek, L. Development of High-Efficiency, Magnetically Separable Palladium-Decorated Manganese-Ferrite Catalyst for Nitrobenzene Hydrogenation. *Int. J. Mol. Sci.* **2022**, *23*, 6535. [CrossRef]
20. Su, T.; Jiang, Y.; Xu, Y.; Luo, X.; Xie, X.; Qin, Z.; Ji, H. Ba-modified Ni-P amorphous alloy/acidified bentonite catalyst: Preparation and the catalytic hydrogenation of nitrobenzene to aniline. *React. Kinet. Mech. Catal.* **2020**, *131*, 805. [CrossRef]

21. Wang, H.; Shi, F.; Pu, M.; Lei, M. Theoretical Study on Nitrobenzene Hydrogenation by N-Doped Carbon-Supported Late Transition Metal Single-Atom Catalysts. *ACS Catal.* **2022**, *12*, 11518. [CrossRef]
22. Wang, W.; Wang, Y.; Zhao, X.; Li, Y.; He, H.; Lian, L.; Zeng, K.; Wu, L.; Deng, L.; Liu, Y.-N. Surface oxygen vacancies of TiO_{2-x} enabled water transfer photocatalytic hydrogenation of nitrobenzene to aniline without use of co-catalyst. *Chem. Eng. Sci.* **2024**, *285*, 119645. [CrossRef]
23. Liu, D.; Nadia, I.; Fang, C.; He, K.; Ge, B.; Chen, H.; Chen, Z. Photo enhanced catalytic activity for hydrogenation of nitrobenzene over Pt-Au/TiO_2 heterojunction. *Appl. Catal. A Gen.* **2022**, *645*, 118840. [CrossRef]
24. Yu, P.; Yang, Z.; Gu, Z.; Wong, H.-W. Catalytic reaction coupling of propane dehydrogenation with nitrobenzene hydrogenation over Pt/Al_2O_3. *Catal. Commun.* **2022**, *166*, 106449. [CrossRef]
25. Jin, M.; Liu, Y.; Zhang, X.; Wang, J.; Zhang, S.; Wang, G.; Zhang, Y.; Yin, H.; Zhang, H.; Zhao, H. Selective electrocatalytic hydrogenation of nitrobenzene over copper-platinum alloying catalysts: Experimental and theoretical studies. *Appl. Catal. B Environ.* **2021**, *298*, 120545. [CrossRef]
26. Xiong, W.; Wang, Z.; He, S.; Hao, F.; Yang, Y.; Lv, Y.; Zhang, W.; Liu, P.; Luo, H. Nitrogen-doped carbon nanotubes as a highly active metal-free catalyst for nitrobenzene hydrogenation. *Appl. Catal. B Environ.* **2020**, *260*, 118105. [CrossRef]
27. Li, C.; Liu, S.; Yang, F.; Zhang, Y.; Gao, Z.; Yuan, X.; Zheng, X. Synthesis of γ-Al_2O_3–supported Pt nanoparticles using Al-based metal-organic framework as medium and their catalytic performance for total propene oxidation and selective nitrobenzene hydrogenation. *Mater. Chem. Phys.* **2020**, *240*, 122146. [CrossRef]
28. Cargnello, M.; Doan-Nguyen, V.V.T.; Gordon, T.R.; Diaz, R.E.; Stach, E.A.; Gorte, R.J.; Fornasiero, P.; Murray, C.B. Control of Metal Nanocrystal Size Reveals Metal-Support Interface Role for Ceria Catalysts. *Science* **2013**, *341*, 771. [CrossRef]
29. Williams, W.D.; Shekhar, M.; Lee, W.-S.; Kispersky, V.; Delgass, W.N.; Ribeiro, F.H.; Kim, S.M.; Stach, E.A.; Miller, J.T.; Allard, L.F. Metallic Corner Atoms in Gold Clusters Supported on Rutile Are the Dominant Active Site during Water—Gas Shift Catalysis. *J. Am. Chem. Soc.* **2010**, *132*, 14018. [CrossRef]
30. Shekhar, M.; Wang, J.; Lee, W.-S.; Williams, W.D.; Kim, S.M.; Stach, E.A.; Miller, J.T.; Delgass, W.N.; Ribeiro, F.H. Size and Support Effects for the Water–Gas Shift Catalysis over Gold Nanoparticles Supported on Model Al_2O_3 and TiO_2. *J. Am. Chem. Soc.* **2012**, *134*, 4700. [CrossRef]
31. Shekhar, M.; Wang, J.; Lee, W.-S.; Cem Akatay, M.; Stach, E.A.; Nicholas Delgass, W.; Ribeiro, F.H. Counting Au catalytic sites for the water–gas shift reaction. *J. Catal.* **2012**, *293*, 94. [CrossRef]
32. Wang, S.; Liu, Y.; Zhao, J. PtN3-Embedded graphene as an efficient catalyst for electrochemical reduction of nitrobenzene to aniline: A theoretical study. *Phys. Chem. Chem. Phys.* **2020**, *22*, 17639. [CrossRef]
33. Shi, Y.; Wang, H.; Wang, Z.; Wu, T.; Song, Y.; Guo, B.; Wu, L. Pt decorated hierarchical Sb_2WO_6 microspheres as a surface functionalized photocatalyst for the visible-light-driven reduction of nitrobenzene to aniline. *J. Mater. Chem. A* **2020**, *8*, 18755. [CrossRef]
34. Zhang, Q.; Bu, J.; Wang, J.; Sun, C.; Zhao, D.; Sheng, G.; Xie, X.; Sun, M.; Yu, L. Highly Efficient Hydrogenation of Nitrobenzene to Aniline over Pt/CeO_2 Catalysts: The Shape Effect of the Support and Key Role of Additional Ce^{3+} Sites. *ACS Catal.* **2020**, *10*, 10350. [CrossRef]
35. Macino, M.; Barnes, A.J.; Althahban, S.M.; Qu, R.; Gibson, E.K.; Morgan, D.J.; Freakley, S.J.; Dimitratos, N.; Kiely, C.J.; Gao, X.; et al. Tuning of catalytic sites in Pt/TiO_2 catalysts for the chemoselective hydrogenation of 3-nitrostyrene. *Nat. Catal.* **2019**, *2*, 873. [CrossRef]
36. LÜ, Z.; Zhu, S.; Dong, M.; Qin, Z.; Fan, W.; Wang, J. Synthesis of γ-Valerolactone through coupling of methyl levulinate hydrogenation with aqueous phase reforming of methanol over Pt/CoxAl catalyst. *J. Fuel Chem. Technol.* **2024**, *52*, 1266. [CrossRef]
37. Dang, T.T.; Pham, V.H.; Vu, B.K.; Hur, S.H.; Shin, E.W.; Kim, E.J.; Chung, J.S. Clean and effective catalytic reduction of graphene oxide using atomic hydrogen spillover on Pt/γ-Al_2O_3 catalyst. *Mater. Lett.* **2012**, *86*, 161. [CrossRef]
38. Lee, S.; Kim, H.; Ryoo, R.; Park, J.Y.; Choi, M. Hydrogen spillover in nonreducible oxides: Mechanism and catalytic utilization. *Nano Res.* **2022**, *15*, 10357. [CrossRef]
39. Hülsey, M.J.; Fung, V.; Hou, X.; Wu, J.; Yan, N. Hydrogen Spillover and Its Relation to Hydrogenation: Observations on Structurally Defined Single-Atom Sites. *Angew. Chem. Int. Ed.* **2022**, *61*, e202208237. [CrossRef]
40. Xing, S.; Xiong, M.; Zhao, S.; Zhang, B.; Qin, Y.; Gao, Z. Improving the Efficiency of Hydrogen Spillover by an Organic Molecular Decoration Strategy for Enhanced Catalytic Hydrogenation Performance. *ACS Catal.* **2023**, *13*, 4003. [CrossRef]
41. Geng, Y.; Li, H. Hydrogen Spillover-Enhanced Heterogeneously Catalyzed Hydrodeoxygenation for Biomass Upgrading. *ChemSusChem* **2022**, *15*, e202102495. [CrossRef] [PubMed]

42. Liu, K.; Yan, P.; Jiang, H.; Xia, Z.; Xu, Z.; Bai, S.; Zhang, Z.C. Silver initiated hydrogen spillover on anatase TiO_2 creates active sites for selective hydrodeoxygenation of guaiacol. *J. Catal.* **2019**, *369*, 396. [CrossRef]
43. Im, J.; Shin, H.; Jang, H.; Kim, H.; Choi, M. Maximizing the catalytic function of hydrogen spillover in platinum-encapsulated aluminosilicates with controlled nanostructures. *Nat. Commun.* **2014**, *5*, 3370. [CrossRef] [PubMed]

Disclaimer/Publisher's Note: The statements, opinions and data contained in all publications are solely those of the individual author(s) and contributor(s) and not of MDPI and/or the editor(s). MDPI and/or the editor(s) disclaim responsibility for any injury to people or property resulting from any ideas, methods, instructions or products referred to in the content.